Mirtron gene therapy for the treatment of rhodopsin-related dominant retinitis pigmentosa

Harry O. Orlans[1,2,3], Michelle E. McClements[1], Alun R. Barnard[1], Cristina Martinez-Fernandez de la Camara[1], Robert E. MacLaren[1,3,4].

1. Nuffield Laboratory of Ophthalmology, University of Oxford, Oxford, UK. 2. St. Thomas' Hospital, London, UK. 3. Moorfields Eye Hospital, London, UK.
4. Oxford Eye Hospital, Oxford, UK.

Background

In the mutation-independent knockdown/replacement treatment paradigm for dominantly-inherited disease, RNA interference (RNAi) may be used to suppress both endogenous alleles of the gene in question (mutant and wild type), whilst RNAi-resistant healthy copies are co-delivered. Mirtrons are atypical RNAi effectors that are spliced from transcripts as introns (Figure 1). We have developed mirtron gene therapy for the mutation-independent treatment of rhodopsin (RHO)-related autosomal dominant retinitis pigmentosa (ADRP), and have demonstrated efficacy in a relevant mammalian model.

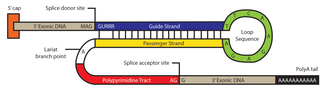


Fig. 1. General molecular structure of 3' tailed mirtrons[1]. The schematic illustrates a 3' tailed mirtron as an intron within a pre-mRNA transcript. The mirtron itself consist of (from 5' to 3'): guide strand, loop sequence (TTCAAGAGA), passenger strand, lariat branch point (A), and polypyrimidine tract. The guide and passenger strands form a hairpin structure through Watson-Crick base pair complementarity, with mismatches being purposefully introduced at the base of the stem to facilitate guide strand selection by the RISC. M = A or C; R = A or G.

Methods

Seven candidate 3'-tailed mirtrons targeting human and mouse rhodopsin were designed *in silico*. Splicing and knockdown efficacy were determined in HEK293 cells (Figs. 2 and 3). Splicing was tested by nesting candidate mirtron sequences within the green fluorescent protein (GFP) gene sequence. Following transfection with these plasmids, green signal would only then be generated by complete and accurate splicing of the nested mirtron sequence. Splicing was further assessed by polymerase chain reaction (PCR) using primers spanning the mirtron. Mirtron-mediated knockdown of rhodopsin was determined *in vitro* by the Dual Glo® assay (Promega). A mirtron-resistant version of the rhodopsin coding sequence was generated using synonymous codons and validated *in vitro* and *in vivo* (Fig. 4). A mirtron-RHO knockdown/replacement adeno-associated virus (AAV), (Fig. 5), was injected subretinally in the *Nrl.GFP/+*, *Rho*$^{P23H/+}$ knock-in mouse model of autosomal dominant retinitis pigmentosa[2]. Rhodopsin RNA replacement was quantified by real-time quantitative PCR in injected retinas (Fig. 6), and the effect of treatment on retinal structure and function determined longitudinally by optical coherence tomography (OCT) and electroretinography (ERG) (Fig.7).

Results

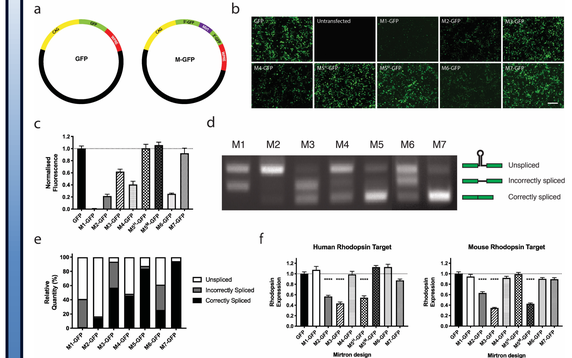


Fig. 2 (above). Splicing efficiency and *in vitro* potency of candidate mirtron designs. a, GFP and Mirtron-GFP plasmid maps. **b,** Fluorescence micrographs of HEK293 cells post-transfection with GFP and M-GFP plasmids. **c,** Fluorescence levels (mean ± SEM) of protein lysates from M-GFP transfected HEK293 samples normalised to that of the GFP-transfected control group (n=3 each). **d,** Representative UV agarose gel image of splice PCR products. The schematic to the right indicates the predicted origin of bands detected. **e,** Relative densitometry of bands corresponding to PCR products derived from a mirtron-spanning primer pair (shown in d). **f,** Determination of mirtron-mediated rhodopsin suppression for human (n=12) and mouse (n=6) rhodopsin targets by the Dual Glo® luciferase assay (Promega, UK).

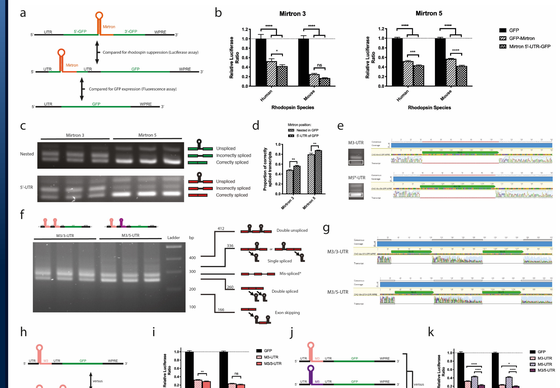


Fig. 3 (bottom left). Splicing and potency of mirtrons located in the 5'-UTR of the *eGFP* transgene. a, Experimental scheme for comparison of nested and 5'-UTR mirtrons in HEK293 cells. **b,** Rhodopsin knockdown compared for 5'-UTR mirtrons and nested equivalents (n=6). **c,** PCR products generated using mirtron-spanning primers and template cDNA derived from cells transfected with nested or 5'-UTR versions of mirtrons. **d,** Band densitometry revealed a greater proportion of correctly spliced transcripts for mirtrons located in the 5'-UTR. **e,** Sanger sequencing of the smallest bands (highlighted in white boxes) confirms accurate splicing of mirtrons from the 5'-UTR. **f,** PCR splice analysis of tandem mirtrons. **g,** Sequencing of the smallest bands in f confirms accurate splicing of tandem mirtrons. **h,** Experimental scheme for comparison of M3-UTR and M3/3-UTR constructs. **i,** Dual Glo® assay comparing M3-UTR and M3/3-UTR (n=12). **j,** Experimental scheme for comparison of M3-UTR, M5-UTR and M3/5-UTR constructs. **k,** Dual Glo® assay comparing M3-UTR, M5-UTR and M3/3-UTR (n>6).

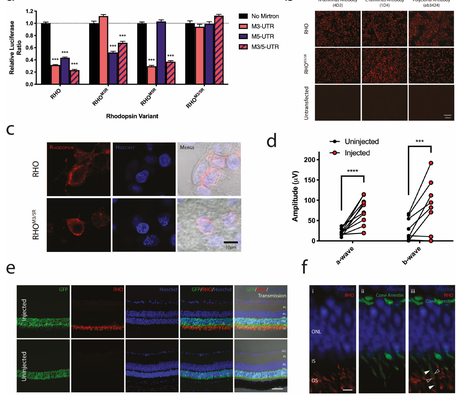


Fig. 4 (above). Codon modification of human rhodopsin. a, Dual Glo® assays demonstrate codon-modification of target regions confers resistance to suppression by the corresponding mirtron(s). n=6. RHO^{M3R}: M3-resistant *RHO*; RHO^{M5R}: M5-resistant *RHO*; RHO$^{M3/5R}$: M3- and M5-resistant *RHO*. **b,** Rhodopsin immunostaining of wild type *RHO*- and codon modified *RHO*$^{M3/5R}$-transfected HEK293 cells. **c,** High magnification view confirming RHO and RHO$^{M3/5R}$ traffic in a similar fashion when expressed in HEK293 cells. **d,** ERG confirms functionality of human transgenic rhodopsin protein expressed from the codon modified *RHO*$^{M3/5R}$ transcript following subretinal delivery of AAV-M3.M5^{H}.RHO$^{M3/5R}$ in rhodopsin-null mice. Dark-adapted a- and b-wave responses of paired uninjected (left) and injected (right) eyes (n=10). **e,** Transgenic human rhodopsin is expressed in rods of *Nrl.GFP/+*, *Rho*$^{-/-}$ mice following subretinal injection of AAV-M3.M5^{H}.RHO$^{M3/5R}$. **f,** High magnification section of an injected retina double stained for rhodopsin and cone arrestin. No overlap of staining was detected confirming restriction of transgenic protein expression to rods. The IS/OS of a single cone stained for cone arrestin (solid arrows) located between two rod OS expressing transgenic human rhodopsin (open arrows) is shown, suggesting rod-specific expression. Scale bar = 20μm.

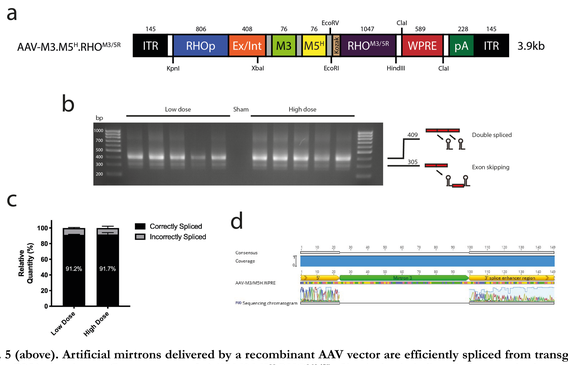


Fig. 5 (above). Artificial mirtrons delivered by a recombinant AAV vector are efficiently spliced from transgenic pre-mRNA *in vivo*. a, Genome map of AAV-M3.M5^{H}.RHO$^{M3/5R}$. Size in bp is indicated above each element and locations of relevant restriction sites marked. Size of the entire genome is shown to the right. ITR: inverted terminal repeat; RHOp: human rhodopsin promoter; Ex/Int: Exon/intron/exon splice site from the CAG promoter; RHO$^{M3/5R}$: codon-modified RHO coding sequence; WPRE: woodchuck hepatitis virus post-transcriptional regulatory element; pA: bovine poly-adenosine signal. **b,** Artificial mirtrons delivered by a recombinant AAV vector are efficiently spliced from transgenic mRNA *in vivo*. DNA gel electrophoresis of amplicons generated using mirtron-spanning primers with template cDNA derived from AAV-M3.M5^{H}.RHO$^{M3/5R}$-injected *Nrl.GFP/+*, *Rho*$^{P23H/+}$ retinas. **c,** Mean relative band density ± SEM for low (2x10^{8}gc) and high dose (2x10^{9}gc) samples (n=5). **d,** Sanger sequencing of DNA extracted from the predominant (larger) band confirmed accurate splicing of the 76bp M3 sequence.

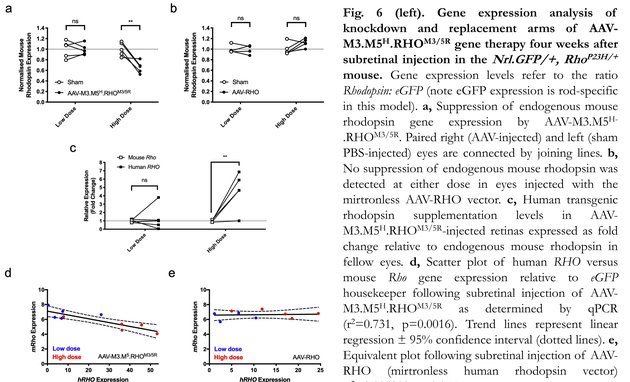


Fig. 6 (left). Gene expression analysis of knockdown and replacement arms of AAV-M3.M5^{H}.RHO$^{M3/5R}$ gene therapy four weeks after subretinal injection in the *Nrl.GFP/+*, *Rho*$^{P23H/+}$ mouse. Gene expression levels refer to the ratio *Rhodopsin*:*eGFP* (note eGFP expression is rod-specific in this model). **a,** Suppression of endogenous mouse rhodopsin gene expression by AAV-M3.M5^{H}.RHO$^{M3/5R}$. Paired right (AAV-injected) and left (sham PBS-injected) eyes are connected by joining lines. **b,** No suppression of endogenous mouse rhodopsin was detected at either dose in eyes injected with the mirtronless AAV-RHO vector. **c,** Human transgenic rhodopsin supplementation levels in AAV-M3.M5^{H}.RHO$^{M3/5R}$-injected retinas expressed as fold change relative to endogenous mouse rhodopsin in fellow eyes. **d,** Scatter plot of human *RHO* versus mouse *Rho* gene expression relative to *eGFP* housekeeper following subretinal injection of AAV-M3.M5^{H}.RHO$^{M3/5R}$ as determined by qPCR (r^2=0.731, p=0.0016). Trend lines represent linear regression ± 95% confidence interval (dotted lines). **e,** Equivalent plot following subretinal injection of AAV-RHO (mirtronless human rhodopsin vector) (r^2=0.005923, p=0.844).

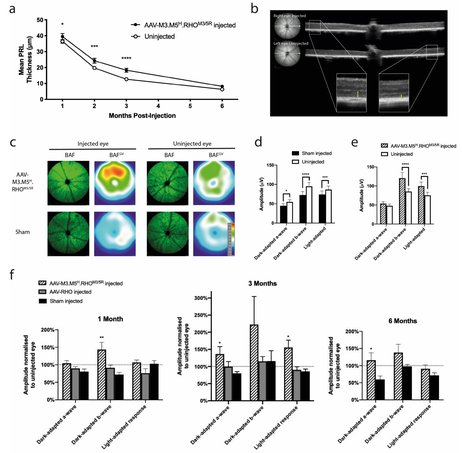


Fig. 7 (above). Partial rescue of retinal degeneration is observed following RNA replacement gene therapy in the rapidly degenerating *Nrl.GFP/+*, *Rho*$^{P23H/+}$ mouse model of ADRP. a, Effect of subretinal injection of 2x10^{8}gc AAV-M3.M5^{H}.RHO$^{M3/5R}$ on photoreceptor layer (PRL) thickness (mean ± SEM; n=17). **b,** Representative SD-OCT images of right (treated) and left (untreated) eyes of a single animal taken one month following subretinal injection of 2x10^{8}gc AAV-M3.M5^{H}.RHO$^{M3/5R}$. **c,** En face cSLO fluorescence imaging of *Nrl.GFP/+*, *Rho*$^{P23H/+}$ retinas following subretinal injection of 2x10^{8}gc AAV-M3.M5^{H}.RHO$^{M3/5R}$ or PBS (sham). Representative blue autofluorescence (BAF) images and BAF mean grey value (BAF^{mGV}) surface plots taken four weeks post-treatment. **d,** Dark-adapted a- and b-wave and light-adapted ERG responses recorded three months after uniocular sham (PBS) injection (n=14). **e,** Equivalent ERG responses recorded three months after uniocular treatment with 2x10^{8}gc AAV-M3.M5^{H}.RHO$^{M3/5R}$ (n=17). **f,** ERG signal of treated eyes normalised to that of fellow untreated eyes at 1-, 3-, and 6-months post-injection.

Conclusions

This represents the first ever demonstration of use of artificial mirtrons for gene therapy *in vivo*. This novel technology could be adapted for the treatment other dominant diseases of the eye and elsewhere.

References

1. Kock, KH, Kong, KW, Hoon, S, Seow, Y. Functional VEGFA knockdown with artificial 3 -tailed mirtrons defined by 5 splice site and branch point. Nucleic Acids Res. 43, 6568–6578 (2015).
2. Orlans HO, Barnard AR, MacLaren RE. Dynamic in vivo quantification of rod photoreceptor degeneration using fluorescent reporter mouse models of retinitis pigmentosa. Exp Eye Res 190: 107895 (2020).

Contact:
harry.orlans@nhs.net

Funding:
MRC Medical Research Council
FIGHT FOR SIGHT The Eye Research Charity
MERTON COLLEGE OXFORD
NUFFIELD DEPARTMENT OF CLINICAL NEUROSCIENCES